Electron scattering from ^{92}Mo

T. E. Milliman, J. P. Connelly, J. H. Heisenberg, F. W. Hersman, and J. E. Wise
Department of Physics, University of New Hampshire, Durham, New Hampshire 03824

C. N. Papanicolas
Department of Physics and Nuclear Physics Laboratory, University of Illinois at Urbana-Champaign, 1110 West Green Street, Urbana, Illinois 61801
(Received 30 October 1989)

Differential cross sections for electron scattering from ^{92}Mo have been measured for excitation energies less than 5.1 MeV over a range of momentum transfer of 0.5 to 3.1 fm^{-1}. The elastic scattering data are analyzed along with existing electron and muonic atom data to provide an improved description of the ground-state charge distribution. The inelastic scattering data have been analyzed to extract electromagnetic transition densities. These densities are interpreted in terms of the underlying nuclear structure.

I. INTRODUCTION

Nuclei in the mass region $N=50$ near the partial proton shell closures of $Z=38$ and 40 provide attractive cases for the study of certain aspects of nuclear structure by electron scattering. Because of the neutron shell closure, the excited states below an excitation energy of 4.0 MeV have approximately the same neutron configuration as the ground state. Excitations primarily involve a relatively small number of protons which are redistributed and recoupled within the valence orbitals to form the excited states. The lack of a significant neutron contribution in the excitation of these states implies that the electromagnetic transition densities determined in an electron scattering experiment contain all the essential structure information.

Ground-state and transition densities are sensitive to the occupations of the orbitals. Multiparticle-multihole configurations are mixed into the ground- and excited-state structure. In addition to the dominant configurations, evidence for polarization of the inner core by transitions between valence levels can be observed and quantified.

The experiment on ^{92}Mo is part of a larger study of several nuclei in this mass region using the (e,e') reaction. A comparison of low-lying quadrupole excitations in ^{88}Sr, ^{89}Y, and ^{90}Zr (Ref. 1) established the strong single-particle nature of these states which had previously been thought to be collective vibrations. A comparison of $E5$ transitions[2] was used to estimate the ground-state occupation of the proton $1g_{9/2}$ orbit. The positive-parity states[3] in ^{90}Zr set the framework for discussing similar states in neighboring isotopes. Early results from the ^{92}Mo experiment[4] have compared the proton $1g_{9/2}$ orbit size in ^{88}Sr, ^{90}Zr, and ^{92}Mo. The interpretation of the ^{92}Mo data presented here will draw heavily from a comparison with the previously studied nuclei.

The increased occupancy of the proton $1g_{9/2}$ orbit motivated the extension of the study to ^{92}Mo. Measurements will be more sensitive to the observables involving this orbit. Comparisons among the current elastic scattering measurements and data from a previous study of ^{90}Zr show charge-density changes from adding two extra protons, nominally to the $1g_{9/2}$ orbit. These protons recouple to angular momentum 2^+, 4^+, 6^+, and 8^+, polarizing the core in the process. Comparisons among these transitions provide a measure of the multipolarity dependence of the core-polarization process. Negative-parity states arise from configurations involving a number of particles changing from the negative-parity f-p orbitals to the $1g_{9/2}$ level or vice versa. Comparisons between the charge and current densities for the 3^- transition indicates a measure of the collectivity. This comparison for the 5^- is used, together with similar data from ^{88}Sr, ^{89}Y, and ^{90}Zr, to determine orbital occupations by examining the ratio of the forward to backward going amplitudes. In the 7^- state, the purity of the configuration allows a determination of the orbital radius and shape. Finally, examination of higher-lying states provides additional spectroscopic and transition density information.

Throughout this paper, in addition to the data-to-data comparisons outlined above, we make comparisons to theory. The shell model contains the valence particle dynamics required to reproduce the spectroscopy. This model provides the conceptual framework and language within which we discuss our results. The broken pair calculation allows effective coupling between low-lying states and the giant resonances, enhancing the strength of transitions. It becomes clear that certain subsets of the experimental observables are reproduced better by each theory.

II. DATA COLLECTION

The data for this experiment was collected on the Energy-Loss Spectrometer System (ELSSY) at the William H. Bates Linear Accelerator Center. No major changes in the data collection facilities occurred while the data were being collected.

A. Experimental facility

The energy was varied in the range of 100–380 MeV. Average currents of 25–35 μA were used. A typical beam structure was 15 μs pulses, with peak currents of 6 mA and a repetition rate of 360 Hz. The signals from two toroids are fed into integrating amplifiers which can measure the beam current to one part in 10^3. The two integrators were periodically calibrated to maintain accuracy.

The 900 MeV/c energy-loss spectrometer[5] was used, with a nominal solid angle of 3.3 msr with a $\pm 3\%$ momentum bite. As part of the current experiment, effort was devoted to a continuing program of resolution enhancement, primarily through data acquisition software refinement and studies of beam tuning systematics. This program resulted in attaining ultimate resolutions of $\Delta p/p = 4\times 10^{-5}$ and routinely gave 6×10^{-5}.

B. Focal plane instrumentation

The focal plane instrumentation consists of two vertical drift chambers[6] (VDC-I and VDC-II), two transverse arrays connected in series (TA), two Čerenkov detectors ($\check{C}1$ and $\check{C}2$), and the associated readout electronics. The instrumentation covers roughly half the spectrometer exit aperture giving a 6% usable momentum bite. The instrumentation is located outside of the vacuum and is separated from the spectrometer vacuum by a thin kevlar-reinforced mylar window.[7] The position of VDC-I corresponds roughly to the position of the focal surface.

C. Targets

This experiment used two molybdenum targets with thicknesses of 5.8 and 19.4 mg/cm^2. The targets were isotopically enriched to 97.4% ^{92}Mo from the natural abundance of 14.8%. In addition to the ^{92}Mo, there were additional targets (either BeO or BeAl), ^{12}C, and at least one other target on which data was being taken. Focal plane parameters and energy calibrations were obtained using excited states and differential recoil from the various nuclides. The ^{12}C targets were also used to help establish normalizations.

III. DATA REDUCTION

A. Extraction of cross sections

Cross sections were extracted from the experimental spectra using the line-shape fitting code ALLFIT.[8] The peak integrals extracted from the spectra were corrected for radiative effects according to the prescription of Bergstrom.[9] In addition, on-line diagnostic spectra were accumulated so that corrections to account for the misidentification of good events and instrumental dead time could be applied. These corrections were normally of the order of a few percent and for the forward-angle data, dominated by the dead-time correction. At backward angles, where the counting rate is low, instrumental dead time is negligible and the correction is dominated by good events corrupted by spurious background events by the computer software. Depending on the amount of background, this correction could be as large as 20% at the backward angles.

Where possible, the data have been normalized to existing high-precision elastic scattering data.[10–12] These data cover a momentum transfer range from 0.5 to 2.1 fm^{-1}. For the forward-angle data, a single normalization factor was fit for each angle sweep using only the data which overlapped with previous measurements. The normalization factors for these data ranged from 0.87 to 1.03. Two methods were used to normalize the backward scattering data. When the elastic peak had sufficient statistics the data point was normalized to forward-angle elastic data. Otherwise a forward-angle measurement was taken and the normalization required for that point was used for the backward-angle data. For the backward-angle scattering the factors ranged from generally 0.82 to 1.14. The data taken at momentum transfers of 0.80 and 0.99 fm^{-1}, however, required normalizations of 1.9 and 0.7 to reach agreement with the existing high-precision elastic scattering data on ^{92}Mo. High data rates are believed responsible for the misidentification of good events for these particular data. Systematic uncertainties due to target thickness and instrumental deadtime of 5–15% were added in quadrature.

B. Transition densities

Several models for transition densities were used to extract structure information from the cross sections. Densities were reconstructed from experimental cross sections in either a Fourier-Bessel expansion (FBE) or a polynomial-times-Gaussian (PG) model. As ^{92}Mo has a closed major neutron shell, many of the low-lying excitations might be expected to have a simple interpretation in terms of one or a few single-proton excitations and we have thus chosen to interpret the extracted densities for many of these levels in terms of a single-particle model (SPM). This density parametrization introduces a strong theoretical bias, unlike the FBE and PG in the reconstruction of the densities, and results derived from it should be understood to reflect this bias.

1. Fourier-Bessel expansion

The FBE expands densities as a series of spherical Bessel functions. The expansions used are

$$\rho(r) = \sum_{\mu=1}^{15} A_\mu q_\mu^{L-1} j_L(q_\mu^{L-1} r) , \tag{3.1}$$

$$J_{L,L+1}(r) = \sum_{\mu=1}^{15} B_\mu j_{L+1}(q_\mu^L r) , \tag{3.2}$$

$$J_{L,L}(r) = \sum_{\mu=1}^{15} C_\mu j_L(q_\mu^L r) , \tag{3.3}$$

where $q_\mu^L R_0$ is the μth zero of $j_L(x)$. The lower components of the current $J_{L,L-1}$ are related to the upper component and the charge through the continuity equa-

tion. For the densities in ^{92}Mo we have used $R_0=11.00$ fm. The data determine the coefficients up to that q_μ^L which is closest to $q_{\max}$, the maximum momentum transfer covered by the data. The remaining coefficients are determined by fitting additional pseudodata points in the region $q_{\max}\le q\le q_{15}^L$, with an uncertainty determined by an exponential upper limit as discussed in Ref. 13. Model dependence enters through the use of an exponential tail bias in coordinate space. The tail bias ensures that the shape of the density is reasonable at large radii.

2. *Polynomial-Gaussian model*

In the PG model the density is expressed as

$$\rho(r)=\sum_{n=1}^{5} A_n (r/r_0)^{2n+l} e^{-(r/r_0)^2} . \tag{3.4}$$

This expansion produces terms which fall off like e^{-r^2} at large r which is the same behavior as harmonic-oscillator wave functions. Up to five terms have been used in the polynomial and the coefficients A_n and the radius parameter r_0 can be fit.

A comparison of PG and FBE fits for the 2_1^+ state in ^{92}Mo revealed that fitting five terms in the polynomial and the radius parameter is sufficient to provide a very good fit. The χ^2 for the PG density is only 2% higher than for the FBE density using 14 coefficients. However, more than in the FBE, the PG expansion with truncation to five terms does introduce a model dependence which can result in poor quality fits. On the other hand, the FBE provides too much flexibility and thus needs to be constrained. This is usually done using a high-q exponential envelope and a tail constraint to prevent unphysical oscillations in the tail of the density. Most of these shortcomings are largely eliminated when the cross section is measured out to a momentum transfer of about twice the Fermi momentum, or about 2.8 fm^{-1}.

3. *Single-particle model*

In the SPM the densities are written in terms of single-particle wave functions. The forms for the densities are given in Ref. 14. The charge density in the SPM is given by

$$\rho_\lambda(r)=\sum_{a,b}\frac{1}{\hat{J}_f} S_\lambda^{ab}\rho_\lambda^{ab}(r) . \tag{3.5}$$

The density is basically a sum over single-particle densities with the spectroscopic amplitudes as weighting factors. The spectroscopic amplitudes are given by

$$S_\lambda^{ab}=\frac{\hat{J}_f}{\hat{\lambda}}\langle \psi_f \| [a_a^\dagger \otimes \bar{a}_b]_\lambda \| \psi_i \rangle . \tag{3.6}$$

The first term in the single-particle density is given by

$$\rho_\lambda^{ab}(r)=eC_\lambda^{ab}u_a(r)u_b(r) \tag{3.7}$$

with

$$C_\lambda^{ab}=(-1)^{\lambda+j_a-1/2}\frac{\hat{j}_a\hat{j}_b}{\sqrt{4\pi}}(j_a\tfrac{1}{2}j_b-\tfrac{1}{2}|\lambda 0) . \tag{3.8}$$

The spin-orbit correction term has been included for the charge density. The current densities can similarly be expressed in terms of the single-particle wave functions and spectroscopic amplitudes. The single-particle wave functions are generated as solutions to a Woods-Saxon well with spin-orbit coupling.

The SPM densities are folded with the nucleon density before comparison with experiment. The procedure for this folding is outlined in Ref. 3, while the nucleon form factors are taken from Refs. 15 and 16. When the transition is dominated by a few particle-hole components, as is often the case for high spin states, this model may provide a good fit with a minimum number of adjustable parameters.

IV. MODEL CALCULATIONS

We compare experimental densities for several levels with calculations from two separate models. Shell-model (SM) calculations were done with the matrix elements and single-particle energies of Haxton and Dubach.[17] These had been generated fitting a residual interaction represented by a combination of a pairing force and a multipole interaction. These matrix elements and energies were applied by Haxton to calculate the excited-state structure of ^{90}Zr and have been applied here to ^{92}Mo without adjustment. The shell-model code used is a descendant of the Glasgow code and uses m-scheme coupling. The neutron shell is assumed closed and only proton excitations among the $1f_{5/2}$, $2p_{3/2}$, $2p_{1/2}$, and $1g_{9/2}$ orbits are allowed. In m-scheme coupling the individual particle couplings are not transparent. The wave functions are given in terms of the occupation numbers for each orbit. In some cases, however, an educated guess of the couplings can be made as will be discussed.

One-broken-pair (BP) calculations were performed by Allaart.[18] A number-projected Bardeen-Cooper-Schrieffer (BCS) ground state was calculated, and excited states built from neutron 1p-1h excitations and proton two-quasiparticle excitations, including participation from the $1f_{7/2}$ through $1h_{11/2}$ orbits. For the calculation of ^{88}Sr and ^{90}Zr some adjustments were made to the single-particle energies to match the energies of some particularly pure 1p-1h high spin states.

Using the one-body spectroscopic amplitudes provided by the microscopic calculations, we have calculated transition densities. To construct the radial shapes of the densities we use wave functions generated with a Hartree-Fock calculation using the density matrix expansion interaction (HF-DME).[19] A SPM expansion for the density then allows a reconstruction of the radial shape. When using the Hartree-Fock (HF) wave functions a correction must be applied for the residual center-of-mass motion of the HF nucleus. This correction is applied using the procedure of Ref. 20. When using the SPM expansion for the density the result must be folded with the nucleon density before comparison with experiment.

The BP and SM calculations address complementary aspects of the nuclear structure issues raised in the study of the extracted densities. The BP calculations give good results for the excitation energies and transition strengths

for states which are predominantly 1p-1h in nature. Since the BP calculation includes a large model space it includes more collectivity (i.e., core polarization) which can significantly increase the strength of the low-lying levels. This is ideal for electron scattering which is only sensitive to the one-body parts of the charge and current operators. The SM calculation, on the other hand, includes the multiparticle-multihole aspects of the structure. The SM provides much better agreement with spectroscopic information at higher excitation energy.

V. RESULTS

We compare the elastic scattering results with the HF-DME calculation of Negele and Vautherin.[19] Figure 1 shows the elastic form factor from a fit to the present data and all previously measured elastic scattering cross sections.

The high-q data (above 2.1 fm^{-1}) collected in this experiment mainly affect the density in the nuclear interior. Figure 2 shows the ground-state density obtained from a fit to the elastic scattering data as well as Barrett moments obtained from an analysis of muonic x-ray transitions.[21] The error bars are significantly reduced in the nuclear interior and the density itself is roughly 10% lower when these high-q data are included. This is outside the one-sigma error bars of the fit done excluding these data and indicates that the incompleteness error is underestimated by the fitting program. This is in agreement with the conclusions of Ref. 22. When the high-q data are included in the fit, the shape of the density more closely resembles the HF-DME prediction also shown in Fig. 2.

A. Charge-density difference

Several elastic scattering studies have examined the difference in ground-state densities between ^{92}Mo and ^{90}Zr.[10–12] Naively the difference should correspond to the density of the additional protons in the orbits to which they are added. For example, the difference in density between ^{92}Mo and ^{90}Zr might correspond to the density of two protons coupled to spin zero in the $1g_{9/2}$ orbit.

Figure 3 shows the difference in the experimental densities between ^{92}Mo and ^{90}Zr. The solid curve is the HF-DME prediction for the density difference. It has been pointed out previously that even though HF calculations may not give an accurate account of the total charge density, such calculations can predict charge-density differences with much higher reliability.[23] We find that the HF-DME prediction gives good agreement in the general shape of the difference and clearly predicts the observed redistribution of the charge out from the nuclear center to the surface region. There remains, however, a serious discrepancy around 2 fm.

The maximum discrepancy occurs where the $2p_{1/2}$

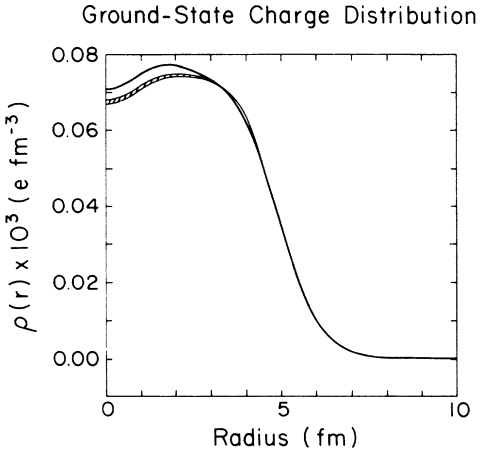

FIG. 2. Fitted ground-state density and associated uncertainty. The solid curve is the HF-DME calculation.

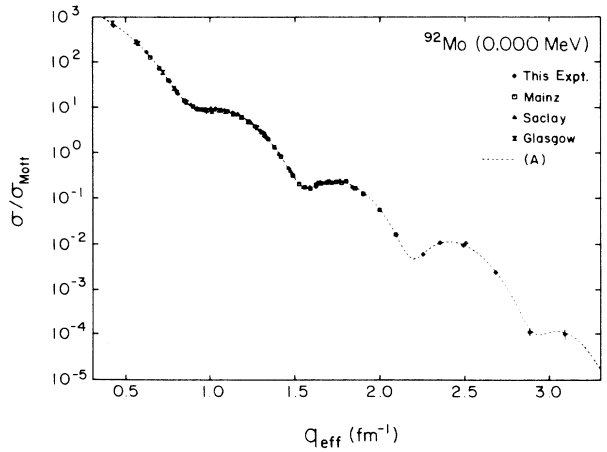

FIG. 1. Elastic scattering form factor showing the ^{92}Mo(e,e') data included in the fit. The data have all been recalculated to 370 MeV. The Mainz data are taken from Ref. 10, the Saclay data are from Ref. 11, and the Glasgow data are from Ref. 12.

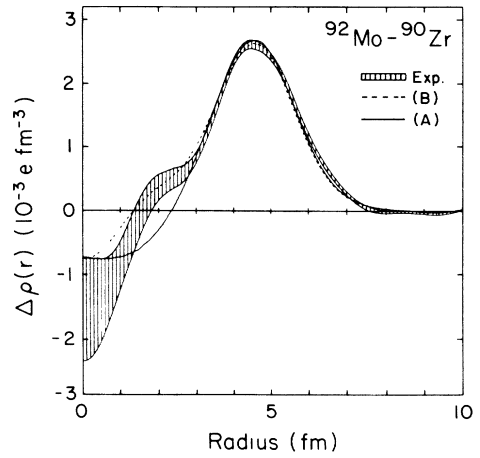

FIG. 3. The difference in the ground-state charge densities between ^{92}Mo and ^{90}Zr. The solid curve is the difference in the HF-DME predictions for the two nuclei. The dashed curve includes the additional occupation in ^{92}Mo of 0.22 proton in the $2p_{1/2}$ orbital.

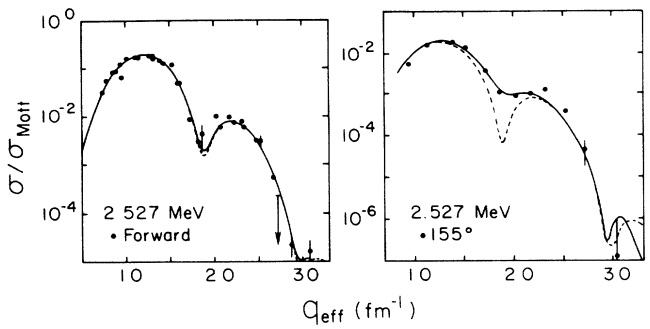

FIG. 4. Form factors for forward and backward scattering angles from the state at 2.527 MeV. The curves are the result of simultaneously fitting the charge and current densities in the FBE. The solid curve is the full fit and the dotted curve is the longitudinal contribution only.

density has a maximum and thus demonstrates that the $2p_{1/2}$ orbit is not yet fully occupied in ^{90}Zr and some charge is being added into this orbit. Because of the pronounced peak in this discrepancy we can use this charge-density difference to determine the amount of charge that has been added into the $2p_{1/2}$ orbit.

This charge-density difference has been modeled using the HF-DME program in the filling approximation, where occupancy factors are multiplied to the density contributions of the various orbitals before variation. The occupancy factors for ^{90}Zr were taken from a recent shell-model calculation. For ^{92}Mo we have added protons into the $2p_{1/2}$ orbit and the $1g_{9/2}$ orbit. The dashed curve shown in Fig. 3 is obtained by adding 0.22 protons into the $2p_{1/2}$ orbit and 1.78 protons into the $1g_{9/2}$ orbit. The excellent agreement obtained with this calculation can be considered as evidence for partial occupancy in these orbits.

B. The $(1g_{9/2}, 2p_{1/2}^{-1})$ 5^- transition

It has been shown previously[2] that one of the main quenching mechanisms in transverse electric excitations is the destructive interference between forward and backward going *ph* excitations. In the pairing model these are related via the quasiparticle transformation to the occupancy of the two orbits involved in the transition. Experimental determination of these quenching factors can thus provide quantitative information on the occupancy of the orbits. This has previously been used to determine the occupation of the $1g_{9/2}$ orbit in ^{90}Zr.

Figure 4 shows the $E5$ form factor for the state at 2.527 MeV. The forward- and backward-angle data were fit simultaneously to extract charge and current transition densities, shown in Fig. 5. The corresponding $E5$ transitions in ^{89}Y (0.909 MeV) and ^{90}Zr (2.319 MeV) have been studied previously. These transitions, which are also shown in Fig. 5, are all dominated by $\pi(1g_{9/2}, 2p_{1/2}^{-1})$ 1p-1h components. In the previous analysis we took the charge and current densities measured in ^{89}Y to be the "effective" single-particle densities for the $\pi(1g_{9/2}, 2p_{1/2}^{-1})$ transition. They are "effective" densities in the sense that any core-polarization or exchange current contributions

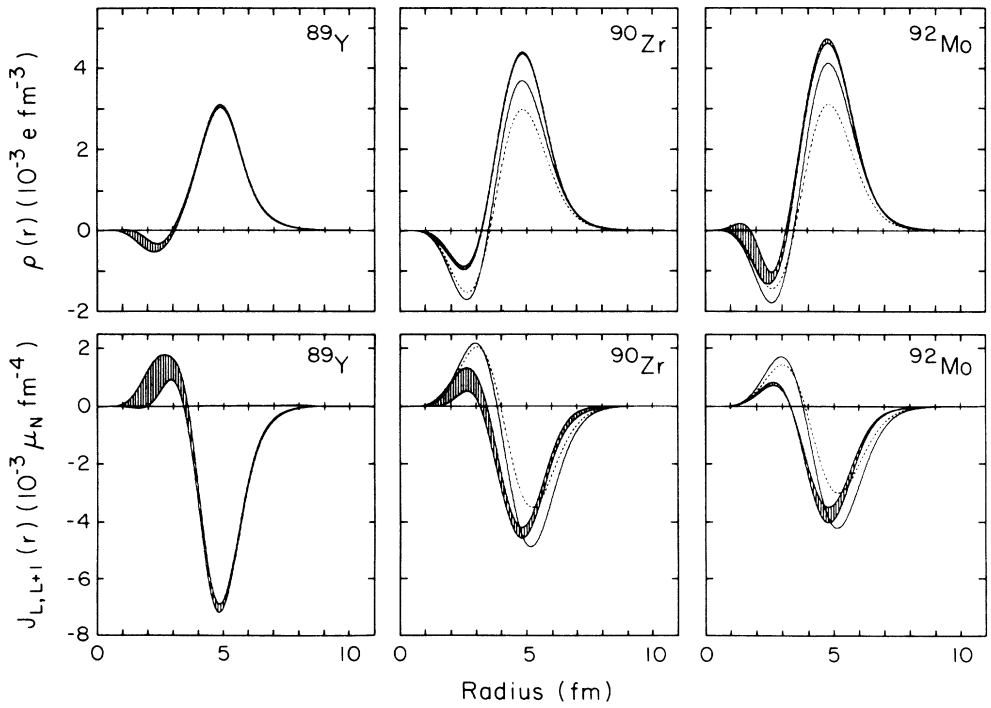

FIG. 5. Transition densities for the $E5$ transitions in ^{89}Y (0.909 MeV), ^{90}Zr (2.319 MeV), and ^{29}Mo (2.527 MeV). The strength of the transition charge increases with Z while the strength of the transition current decreases. The solid curves are the BP predictions and the dashed curves are the predictions of the SM calculation.

are included. Both of these contributions should vary only slowly with particle number and therefore be roughly the same in ^{90}Zr and ^{92}Mo as in ^{89}Y.

A comparison of these densities dramatically illustrates the previously reported quenching of the transition current with respect to the transition charge. In the HF picture the $2p_{1/2}$ orbit should be filled and thus the additional protons in the $1g_{9/2}$ orbit should cause Pauli blocking leading to a reduced strength of this transition in ^{92}Mo. The opposite is observed. This demonstrates that in going from ^{90}Zr to ^{92}Mo the occupation in the $2p_{1/2}$ orbit increases, compensating for the additional blocking.

While the transition charge increases with Z, the transition current decreases. Scaling the effective charge density from ^{89}Y to fit the density in ^{90}Zr or ^{92}Mo would lead to an over prediction in the current density. This quenching has been interpreted as being due to the presence of backward going $\pi(2p_{1/2}, 1g_{9/2}^{-1})$ components. In the BCS model, the densities for a two-quasiparticle excitation are given as

$$\tilde{\rho}_\lambda^{ph}(r)=(u_p v_h+v_p u_h)\rho_\lambda^{ph}(r) ,$$

$$\tilde{J}_\lambda^{ph}(r)=(u_p v_h-v_p u_h)J_\lambda^{ph}(r) .$$

The forward going amplitude, $u_p v_h$, and backward going amplitude, $v_p u_h$, add in the charge density and subtract in the current density. An increase in the backward going amplitudes as the occupation of the $\pi 1g_{9/2}$ orbit increases from ^{89}Y to ^{92}Mo does explain the behavior seen in Fig. 5. (The situation as described applies to even-even nuclei only. For odd-even nuclei the backward going, i.e., time-reversed, component has the opposite sign in both the charge and current. We apply the appropriate equations for the pairing factors to the odd-even nucleus ^{89}Y.)

If we assume this mechanism for the quenching we can calculate the ratio of the backward to forward going amplitudes. The occupations of the orbits can also be estimated since $v^2=1-u^2$ is the occupation probability of an orbit.

We can write

$$\rho_Y(r)=(A+\bar{A})\rho_{p\to g}(r),\quad J_Y(r)=(A-\bar{A})J_{p\to g}(r) ,$$

$$\rho_{Zr}(r)=(B+\bar{B})\rho_{p\to g}(r),\quad J_{Zr}(r)=(B-\bar{B})J_{p\to g}(r) ,$$

$$\rho_{Mo}(r)=(C+\bar{C})\rho_{p\to g}(r),\quad J_{Mo}(r)=(C-\bar{C})J_{p\to g}(r) .$$

Then the ratios at a given radius can be written

$$R_{Zr}=\left[\frac{\rho_{Zr}}{\rho_Y}\right]\left[\frac{J_Y}{J_{Zr}}\right]=\frac{(A-\bar{A})}{(A+\bar{A})}\frac{(B+\bar{B})}{(B-\bar{B})} .$$

Similarly we get

$$R_{Mo}=\left[\frac{\rho_{Mo}}{\rho_Y}\right]\left[\frac{J_Y}{J_{Mo}}\right]=\frac{(A-\bar{A})}{(A+\bar{A})}\frac{(C+\bar{C})}{(C-\bar{C})} .$$

Taking the ratios from the maximum values of the measured densities gives

$$R_{Zr}=2.3\pm0.1$$

and

$$R_{Mo}=2.9\pm0.2 .$$

If the ^{89}Y ground-state occupation of the $2p_{1/2}$ is taken at 1.0 ± 0.1 proton, and the ratio $\bar{A}/A=-0.07\pm0.007$ is taken from a shell-model calculation for ^{89}Y (Ref. 24), the ratios for ^{90}Zr and ^{92}Mo are found to be

$$\frac{\bar{B}}{B}=0.34\pm0.08$$

and

$$\frac{\bar{C}}{C}=0.44\pm0.08 .$$

To estimate the occupation of the $\pi 1g_{9/2}$ orbit in ^{90}Zr we take the value of $v_h^2=0.63$ as determined in transfer reactions.[25,26] From this and the ratio $\bar{B}/B$ one gets

$$v_p^2=0.16\pm0.05 .$$

For ^{92}Mo one can assume that the total number of protons in the $2p$ and $1g$ orbits is two more than was found for ^{90}Zr. This is equivalent to assuming that the depopulation of the $1f_{5/2}$ and $2p_{3/2}$ orbits is about the same in ^{90}Zr as in ^{92}Mo. This constraint can be written as

$$2v_h^2+10v_p^2=4.9\pm0.6$$

and gives the values

$$v_p^2=0.34\pm0.07$$

and

$$v_h^2=0.74\pm0.2 .$$

Simple error propagation has been used in this analysis. Errors from the measured ratios have been used along with an estimated 10% error for the value of the ratio $\bar{A}/A$ in ^{89}Y and a 2% error on the occupancy of the $2p_{1/2}$ orbit in ^{89}Y. This estimate is based on recent shell-model[27] calculations which give the occupancy of the $2p_{1/2}$ orbital in ^{89}Y as 0.98 ± 0.01 when averaged over the results of calculations varying in the parameters of the effective interaction. Determinations of the emptiness probability and occupation probabilities taken with stripping and pickup reactions for the ^{90}Zr $2p_{1/2}$ orbit gives a total probability of $u^2+v^2=1.07$. We give an error of 10% to this value.

To estimate the model error we have performed shell-model calculations to predict the BCS pairing factors for the $E5$ transition in ^{90}Zr. These calculations give $u_p v_h=0.803$ and $u_h v_p=0.233$. Our values from the $E5$ quenching analysis for these quantities are 0.805 and 0.179, respectively. This represents a maximum of a 23% deviation that we attribute to our assumption that BCS provides a valid description for these transitions. This model error should be added to the results of the error propagation analysis given above.

Calculating these occupations from the quenching factors serves a dual purpose. It is a test of the proposed quenching mechanism (i.e., the backward going amplitudes) by checking its consistency with transfer reactions.

TABLE I. Summary of information on the occupation of the $\pi 1g_{9/2}$ orbit in $N=50$ nuclei. The $E5$ quenching analysis labeled (a) uses the occupation probability for the $2p_{1/2}$ orbital in ^{90}Zr as measured from transfer experiments while (b) is based on the $(e,e'p)$ knockout data.

	Number of protons in the $\pi 1g_{9/2}$ orbit					
Nucleus	Transfer reactions	$(e,e'p)$ reactions	$E5$ quenching analysis (a)	$E5$ quenching analysis (b)	Broken pair (BP)	Shell model (SM)
^{88}Sr					1.04	0.27
^{89}Y			0.05(1)	0.05(1)		0.18
^{90}Zr	1.1	0.54(5)	1.63(49)	0.63(16)	1.64	1.13
^{92}Mo	3.4		3.42(66)	2.18(15)	3.18	2.83

The quenching data also represents an independent (although model-dependent) measurement of some of the occupations. We can compare the occupations obtained in this way with the results of transfer reactions and also with spectroscopic amplitudes from the previous section. Table I contains a summary of information on the occupation of the $\pi 1g_{9/2}$ orbit for several nuclei. The numbers for transfer reactions are averages over several measurements.[25,28–31] In general, the estimates from the quenching factors are consistent with the transfer reactions. For ^{90}Zr the occupation from quenching is higher than the average from the transfer reactions but there is considerable variation among the different measurements. However, it should be noted that the occupations taken for the orbits from transfer reactions are considerably larger than would be indicated from the ^{90}Zr $(e,e'p)$ ^{89}Y knockout data of den Herder.[32] If we use the value obtained in that measurement of 0.36 ± 0.04 for the occupation probability of the $2p_{1/2}$ orbit in ^{90}Zr, we obtain an occupation for the ^{90}Zr $1g_{9/2}$ orbit of 0.63 ± 0.16 protons from our $E5$ quenching analysis. This value is consistent with the value of 0.54 ± 0.05 measured in that experiment for the $1g_{9/2}$ occupation, but is low as compared to the transfer reaction experiments and theoretical calculations. This illustrates that we are sensitive to the relative occupations only, and our results for the absolute values of the occupations are dependent on our initial assumptions for the occupations of the hole orbits.

It is also interesting to examine the measured spectroscopic amplitudes for the $E8$ transitions (shown in Table II) with the values predicted by the two calculations. In particular, it would be interesting to relate the amplitudes to ground-state occupations. Unfortunately there is a large model dependence when connecting the amplitudes to occupations. The SM calculation has virtually the same spectroscopic amplitude as the BP calculation but an occupation of 2.83 protons in the $\pi 1g_{9/2}$ orbit. While the amplitudes do not serve as quantitative indicators of occupation they certainly must be consistent with the occupations observed. The good agreement between the ^{90}Zr and ^{92}Mo BP amplitudes with the transfer experiment indicates that this calculation is consistent with relatively large occupations in this orbit. The SM calculation has lower $1g_{9/2}$ occupations for all these nuclei, though not as low as seen in the $(e,e'p)$ experiment.

TABLE II. Summary of data on 8^+ states in ^{88}Sr, ^{90}Zr, and ^{92}Mo.

	Comparative study of 8^+ states			
Nucleus	r_{rms} (fm)	S_8^{gg}	S_8^{gg} (BP)	S_8^{gg} (SM)
^{88}Sr	4.95±0.07	0.360±0.015	0.339	0.198
^{90}Zr	5.04±0.04	0.410±0.004	0.442	0.431
^{92}Mo	5.06±0.04	0.582±0.010	0.678	0.667

C. The $\pi(1g_{9/2}^2)$ multiplet

The low-lying positive-parity states form a $2^+,4^+,6^+,8^+$ multiplet based on the $\pi(1g_{9/2}^2)$ configuration. The same multiplet has been observed in ^{90}Zr as have the 6^+ and 8^+ states in ^{88}Sr. Figure 6 shows the excitation energies of the states attributed to this configuration in ^{88}Sr, ^{90}Zr, and ^{92}Mo. The excitation of these states by electron scattering indicates the presence of $\pi(1g_{9/2}^2)_{0^+}$ components in the ground states of these nuclei. The data for ^{90}Zr and ^{88}Sr have been previously reported in Refs. 3 and 33.

The form factors for the states in ^{92}Mo are shown in Fig. 7. For the 2^+ state, the $B(E2)$ value of $1.13\pm0.06\times10^3$ e^2 fm^4 as determined in Coulomb excitation measurements[34] was included in the fit as an extra data point. The backward-angle scattering data for these

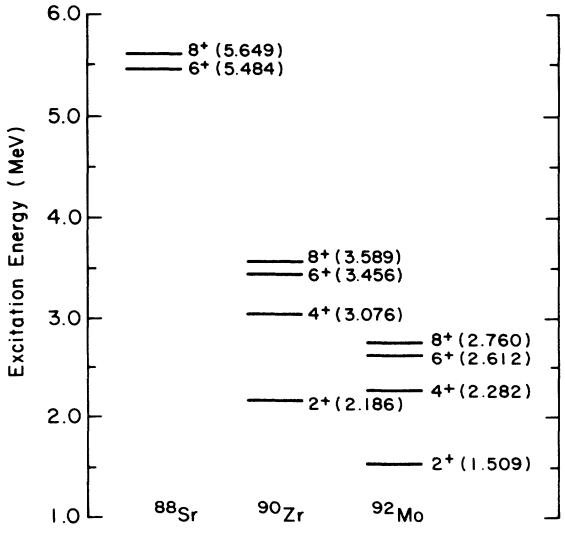

FIG. 6. Excitation energies of states attributed to the $\pi(1g_{9/2})^2$ configuration.

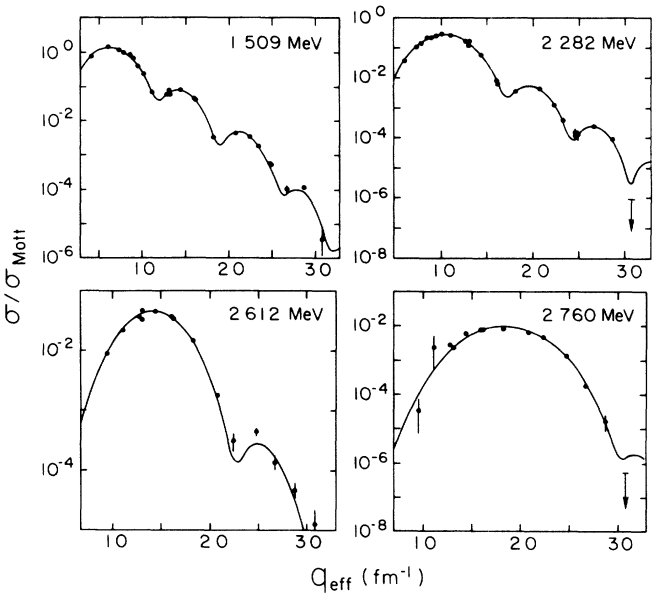

FIG. 7. Forward-angle scattering data for the positive-parity states based on the $\pi(1g_{9/2}^2)$ multiplet. Form factors for the states at 1.509 MeV (2^+), 2.282 MeV (4^+), 2.612 MeV (6^+), and 2.760 MeV (8^+) in ^{92}Mo are shown. The curves showing the DWBA fits are discussed in the text.

levels are well fit using the density obtained by fitting the forward scattering data alone. This indicates only a negligible contribution from the transition current density as is expected for recoupling of a proton pair. For the 2^+ and 4^+ states, the fit was done using the FBE for the density. For the 6^+ state, the fit was done using the SPM with a density of the form

$$\alpha\pi(1g_{9/2},1g_{9/2}^{-1})+\beta\pi(2d_{5/2},1g_{9/2}^{-1}) .$$

The two amplitudes α and β were fitted while the radius parameter was kept fixed at a value determined in the 8^+ fit (1.332 fm). The fit gave values of $\alpha=0.685$ and $\beta=0.113$. For the 8^+ state, the SPM was used with a single component, $\pi(1g_{9/2},1g_{9/2}^{-1})$ in the density. For the 8^+ state, both the $1g_{9/2}$ radius and the amplitude were fitted. The results of this fit are shown in Table II.

If these states were pure $(1g_{9/2}^2)$ configurations the strength of the transitions would be correlated to the $1g_{9/2}$ occupation in the ground state. The shape of the density would likewise be determined by the shape of the $1g_{9/2}$ radial wave function. Usually, however, the lowest excited states of a given multipolarity are highly collective. To use these states to obtain spectroscopic information one must first understand the collective aspects of their structure.

In Ref. 3 a shell-model plus core-polarization calculation for the multiplet in ^{90}Zr is shown. It indicates that the contribution from core polarization decreases as the spin increases. This is a result of two factors: fewer 1p-1h combinations can couple to form the higher spin states, and the residual interaction used in the calculation has a finite-range attractive component balanced by a zero-range repulsive component. In q space the repulsive part is constant while the attractive part decreases with q. States with higher spin sample the interaction at larger values of q and therefore see a much weaker residual interaction. This effect also contributes to the energy splitting of the multiplet.

The transition densities for this multiplet provide a good observable to test models which include both the individual particle and collective aspects of the nuclear structure in this region. Also shown in Fig. 8 are the predictions of the two calculations, SM and BP. While both calculations do a reasonable job of predicting the excitation energies of these states and predict the shapes of the densities well, quantitative agreement with the experimental densities is lacking. It is interesting to note that the largest disagreements between theory and measurement occurs for the 2^+ and 8^+ states. For the 2^+ state,

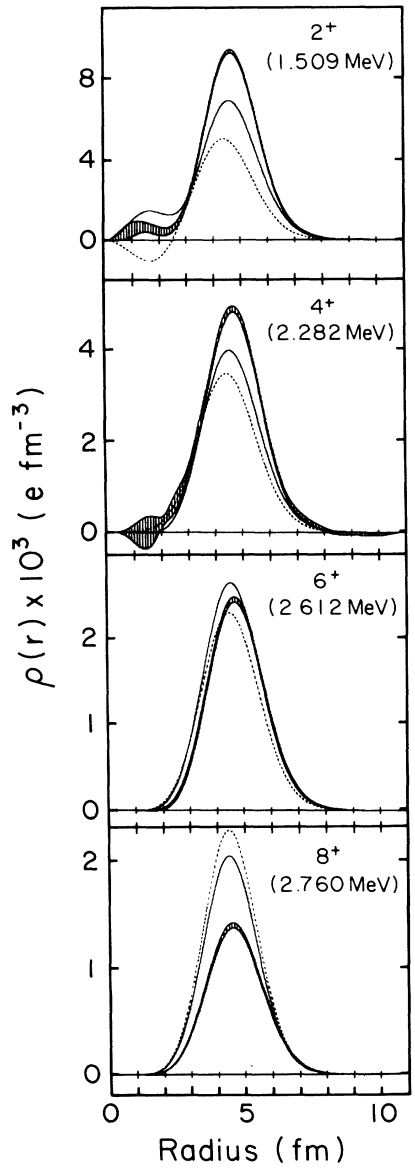

FIG. 8. Transition charge densities for the $2^+,4^+,6^+,8^+$ multiplet due to the $\pi(1g_{9/2}^2)$ configuration.

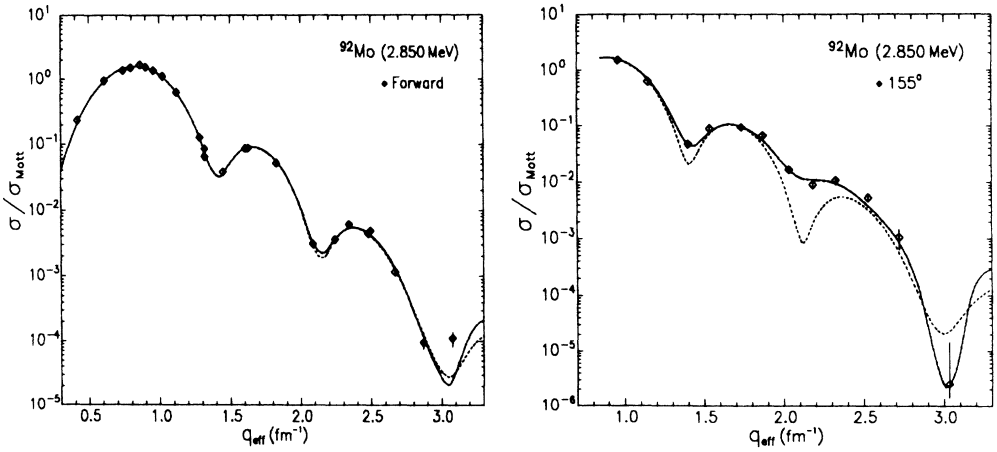

FIG. 9. Forward- and backward-angle scattering data for the 3^- level at 2.850 MeV. The solid curve is the full DWBA fit to the data while the dashed curve gives the longitudinal contribution only.

both calculations lack enough collectivity to account for the large strength. As would be expected, the BP calculation with the much larger model space does a better job. For the 8^+ state, however, there should be very little collectivity. Here the two calculations are in fairly close agreement but both predict too much strength.

We can use the results of the BP calculation to obtain a value for the ground-state occupation based upon our measured result for the amplitude of the $(1g_{9/2}^2)$ configuration in the 8^+ state. Interpolating between the results of the amplitude obtained in the BP calculation for the $(1g_{9/2}^2)$ component for the 8^+ excitation from both ^{90}Zr and ^{92}Mo, we find the occupancy of the ground state to be 2.5 ± 0.1 protons from our experimental result. This result is closer to the $E5$ quenching analysis based upon the $(e,e'p)$ spectroscopic factors, though still some 15% higher than anticipated from that analysis. Clearly more realistic models of the nuclear structure are needed to provide accurate estimates of the ^{92}Mo occupations based upon the present data.

D. The 3^- state at 2.850 MeV

The nuclei ^{88}Sr, ^{90}Zr, and ^{92}Mo each have a strongly excited 3^- state at low excitation energy (2.734, 2.748, and 2.850 MeV, respectively). The similarity in excitation energy and transition strength of these levels indicates that they are relatively independent of proton number and are collective in nature. The states in ^{90}Zr and ^{92}Mo have been previously studied in a comparison of collective levels in isotone pairs.[35] The present measurement has an order of magnitude better resolution and extends the data to higher momentum transfer.

Figure 9 shows the form factor for the 3^- level in ^{92}Mo. A Fourier-Bessel analysis of the charge and current densities was performed by a simultaneuous fit to the forward- and backward-angle scattering data in DWBA. The resulting densities are shown in Fig. 10. The dashed curve in Fig. 9 shows the contribution from the charge scattering alone. The difference shows that the contribution of the current is especially important

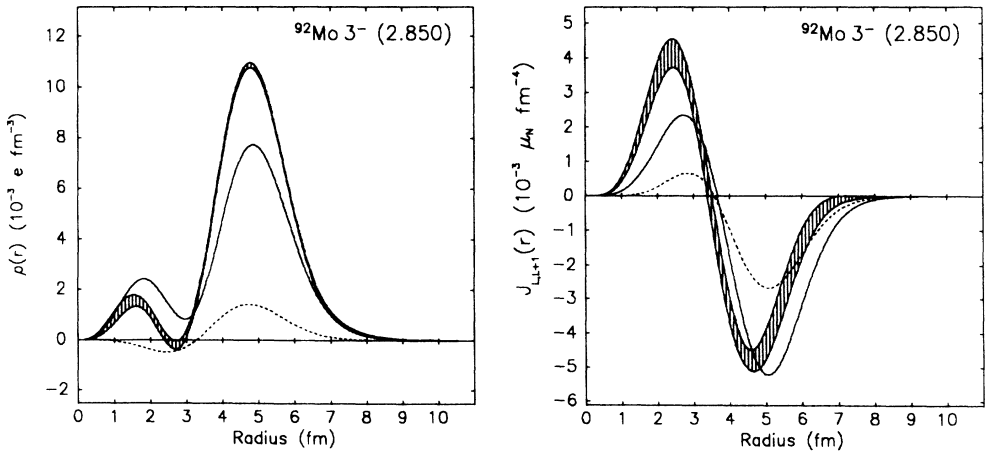

FIG. 10. Transition charge and current densities for the 3^- state at 2.850 MeV. The solid curve is the BP prediction while the dashed curve is the SM calculation.

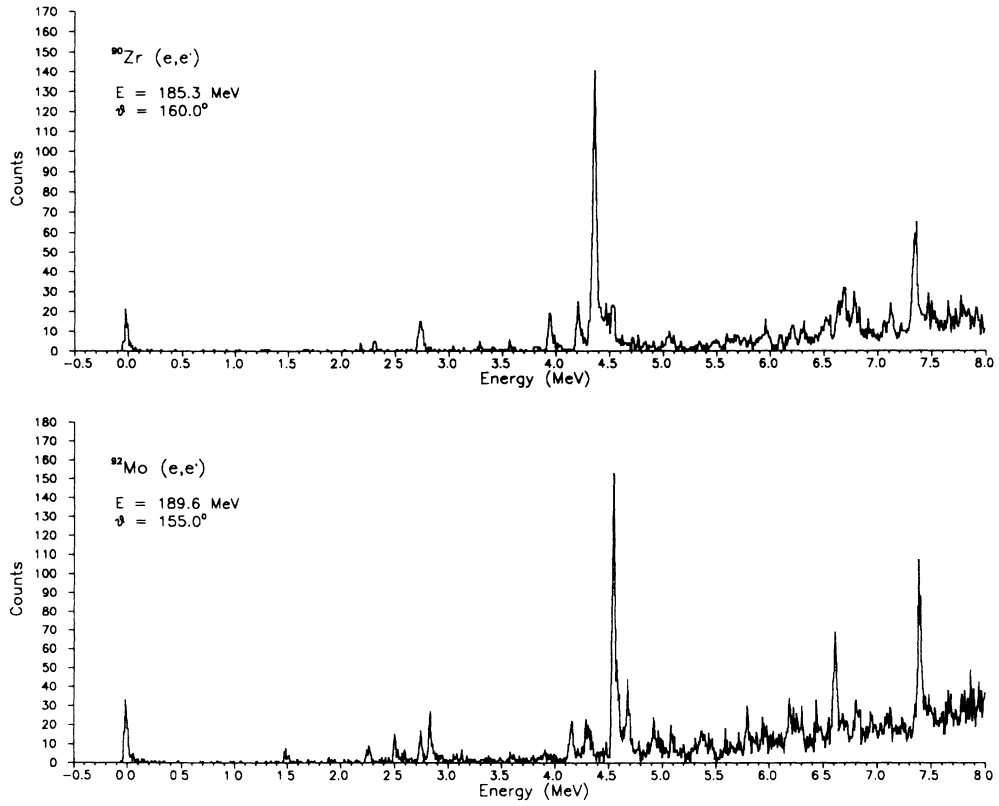

FIG. 11. Spectra of electrons scattered from ^{90}Zr (top) and ^{92}Mo (bottom) at backward scattering angles. The momentum transfer of the two spectra have roughly the same value. The strong 7^- states stand out clearly at the backward angles and higher momentum transfers.

near the minimum of the charge form factor. In ^{88}Sr a current density was also measured. For ^{90}Zr the measurement of a current density was made impossible by the presence of an unresolved 4^- state at 2.476 MeV.

Because the 3^- level is thought to be highly collective, the presence of any transverse strength is somewhat surprising. The collective 3^- state in ^{208}Pb has been shown to have very little transverse strength beyond that required by Siegert's theorem. As discussed in Ref. 13, the absence of the current $J_{L,L+1}$ is a feature of collective states. This is equivalent to assuming that the nuclear motion can be described as the irrotational flow of an incompressible fluid. While this assumption appears to be valid for heavier nuclei, in the mass-90 region it is not.

The BP calculation is also shown in Fig. 10. The transition charge density is underpredicted as is expected for

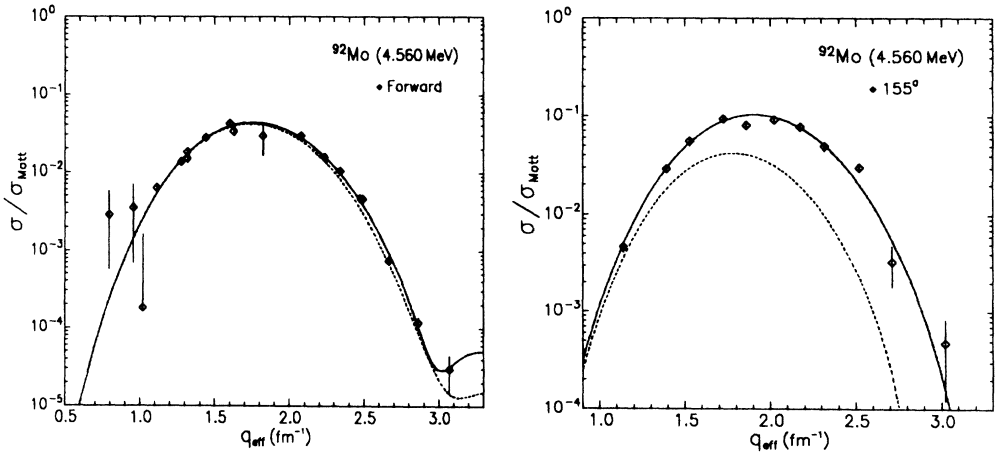

FIG. 12. Forward and backward scattering form factors for the 7^- state at 4.555 MeV. The solid curve is the full DWBA fit. The dashed curve gives the longitudinal contribution only.

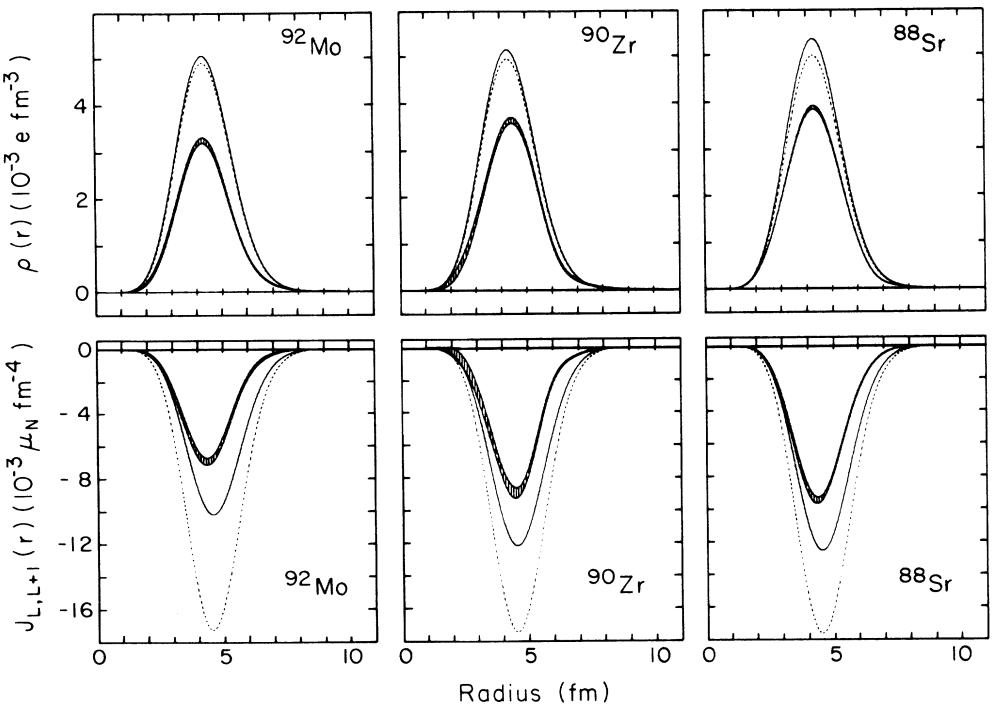

FIG. 13. The transition charge and current densities for the 7^- states in ^{88}Sr (4.366 MeV), ^{90}Zr (4.373 MeV), and ^{92}Mo (4.555 MeV). The solid curve is the BP prediction. The dashed curve is the prediction of a pure single-particle transition.

a highly collective level. The current density, however, is in remarkable agreement with the measured density. The dominant component of the calculated transition current is $\pi(1g_{9/2},2p_{3/2}^{-1})$. The first 3^- states in ^{88}Sr and ^{92}Mo therefore appear to have a combination of a strong single-particle component and large core polarization. While the excitation energy and transition charge density provide information on the collective aspects of the structure, the shape and strength of the transition current reveals single-particle aspects of the structure. This further illustrates the point that the underlying nuclear structure is better understood by a determination of both the transition charge and current densities than by a determination of the transition charge density alone.

E. The 7^- state at 4.555 MeV

The 5_1^- and 3_1^- states have strong $\pi(1g_{9/2},2p_{1/2}^{-1})$ and $\pi(1g_{9/2},2p_{3/2}^{-1})$ components, respectively. A similar state with a strong single-particle nature should exist with a $\pi(1g_{9/2},1f_{5/2}^{-1})$ component. In ^{88}Sr and ^{90}Zr 7^- states corresponding to this configuration have been identified at 4.366 and 4.370 MeV, respectively.

In previous reactions on ^{92}Mo a state of unknown spin and parity has been observed at 4.555-MeV excitation. In the (e,e') reaction a state at this energy can be identified with the stretched $f\rightarrow g$ configuration similar to the 7^- states observed in ^{88}Sr and ^{90}Zr. Figure 11 shows a backward scattering electron spectrum taken for ^{90}Zr and ^{92}Mo at roughly the same momentum transfer. The close resemblance between the two spectra made the location of the 7^- state particularly easy.

Figure 12 shows the form factor and fit for the 4.555-MeV state in ^{92}Mo. The forward and backward scattering data were fit simultaneously in FBE to extract the charge and current transition densities. These densities are shown in Fig. 13. Also shown are the BP predictions and a pure single-particle prediction using the $\pi(1g_{9/2},1f_{5/2}^{-1})$ configuration.

In ^{88}Sr, ^{90}Zr, and ^{92}Mo the $E7$ strength observed is considerably less than for a pure particle-hole transition. Relative to the single-particle prediction, the maximum of the transition charge densities are quenched by 0.77, 0.73, and 0.66, respectively. This situation is surprising and as yet unexplained. One possible explanation is that configuration mixing causes the strength to be spread out over several levels. This explanation seems unlikely for two reasons. First in ^{88}Sr the 4.366-MeV state is the

TABLE III. Radius of the $\pi 1f_{5/2}$ orbit determined by fitting the $E7$ form factors in ^{92}Mo.

	$\pi 1f_{5/2}$ orbit radius determination			
	Single radius	Separate radii fit		
Nucleus	fit	Charge	Current	Δ
^{92}Mo	4.28±0.09 fm	4.35±0.08 fm	3.95±0.10 fm	0.40±0.06 fm

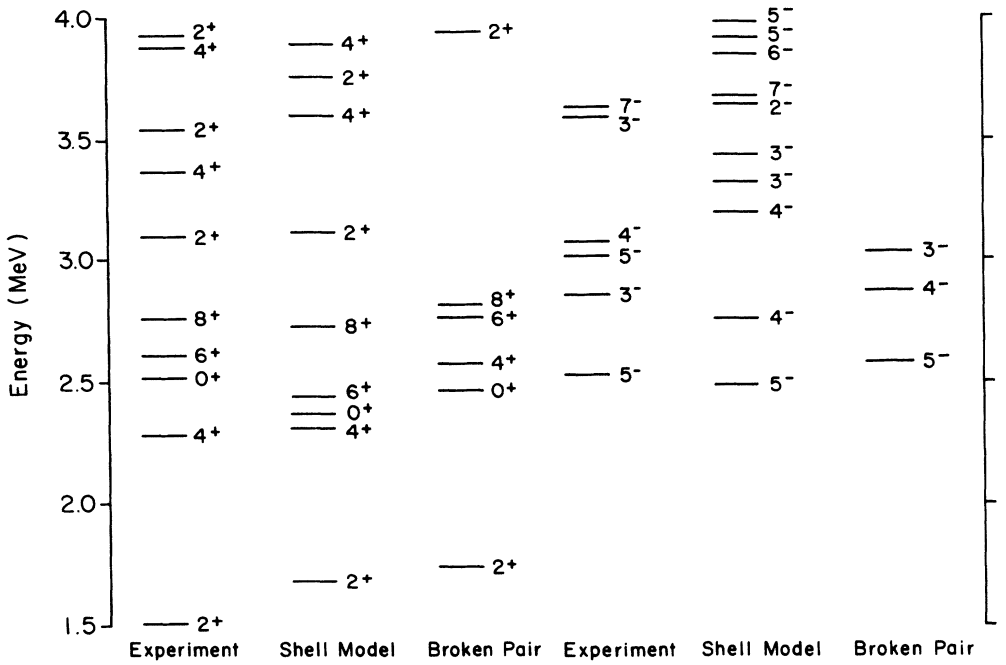

FIG. 14. The known excited states in ^{92}Mo below 4.0 MeV and the predictions of two calculations.

lowest known 7^- state. Usually the configuration mixing tends to enhance the transition charge density for the lowest level of a given multipolarity. Instead there is a reduction of roughly 20%. Secondly, in ^{92}Mo where there is another known 7^- state at a lower energy (3.626 MeV), it has very little single-particle strength. This state will be discussed in more detail in a later section.

In addition to the density fit described above, a fit was done using the SPM with a single component, $\pi(1g_{9/2}, 1f_{5/2}^{-1})$, for the density. Because the transitions mainly involve two single-particle orbits, $\pi 1f_{5/2}$ and $\pi 1g_{9/2}$, the results of the fits can provide detailed information on the radial shapes of the wave functions. Since the shapes of the $\pi 1g_{9/2}$ orbits have already been established by studying the 8^+ transitions, the fits to the $E7$ transitions depend only on the shape of the $\pi 1f_{5/2}$ orbit.

In the SPM fit, Woods-Saxon wave functions were used with a fixed diffuseness parameter of 0.70 fm and spin-orbit strength of 7.50 MeV. The separation energies were 8.96 MeV for the $\pi 1f_{5/2}$ orbit and 6.05 MeV for the $\pi 1g_{9/2}$ orbit. The $\pi 1f_{5/2}$ radius was left as an adjustable parameter and was fit to the data along with the transition amplitude. The fit was done simultaneously to forward and backward scattering data. The χ^2 for this fit was much worse than the fit using an FBE model for the density. To improve the fit the densities were constructed so that different $\pi 1f_{5/2}$ wave functions were used for the charge and current densities and the two radius pa-

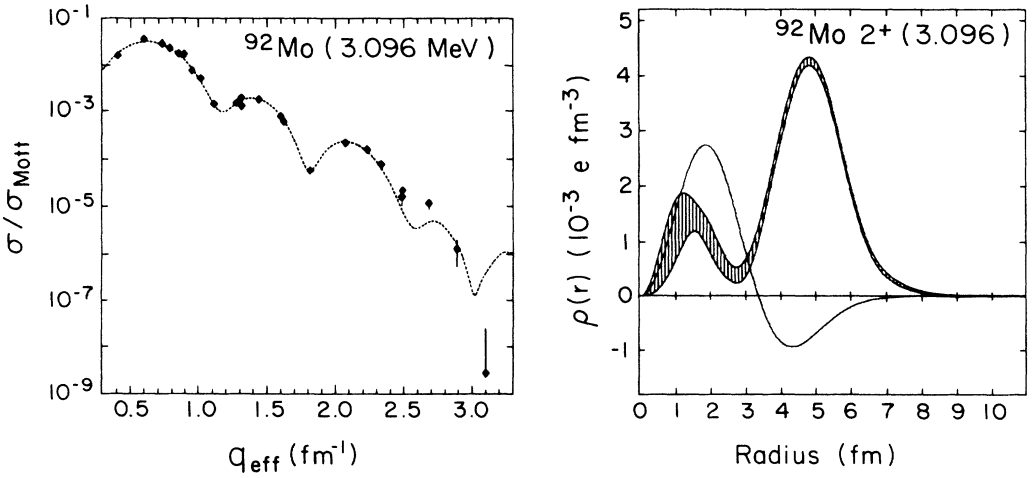

FIG. 15. Form factor and transition charge density for the second 2^+ state at 3.092 MeV.

rameters were fit. In this manner a good fit was obtained comparable to the FBE fit. The radii determined in these fits are shown in Table III. In addition to the statistical uncertainties, the quoted uncertainties include contributions from varying the fixed parameters. For the fixed parameters a variation of 10% in the diffuseness parameter and spin-orbit strength was included along with a 1.5-MeV variation of the separation energies.

A surprising feature of the densities is found. Table III shows the results of fitting the full data set and fitting separately the forward and backward scattering data. The fitted radius for the forward scattering data is significantly larger than the radius fit for the backward scattering data. The sum of the χ^2's for the separate fits is about half of the χ^2 for the combined fit indicating a much better fit if different radii are used for the longitudinal and transverse components. While about half the uncertainty of the radius values comes from uncertainty in the fixed parameters, the uncertainty in the difference of the radii is dominated by the statistical uncertainty. This indicates that it is really the data which are determining this quantity.

While still unexplained, these results appear to be consistent with other observations involving orbit radii. In the study of the $\pi 1g_{9/2}$ radial shape it was noted that the rms radius obtained for ^{93}Nb from a magnetic elastic scattering experiment[36] was considerably smaller than the orbit radii for either ^{90}Zr or ^{92}Mo obtained from fitting the 8^+ form factors. The magnetic scattering is sensitive mainly to the magnetization current of the unpaired nucleon while the 8^+ measurement involves only the transition charge density. A similar study[37] of the $1f_{7/2}$ orbit was made by comparing the results of scattering from ^{50}Ti, and ^{51}V showed again that a much smaller radius was needed to explain the magnetic scattering data. The difference in radius between the charge and magnetic scattering obtained in the results from Ref. 37 are in good agreement with the results found here. In that experiment, the $\pi 1f_{7/2}$ orbit was found to have a radius of 4.29 ± 0.03 fm for the charge scattering and 4.06 ± 0.05 fm for magnetic scattering. The present results for the $E7$ transitions are particularly interesting in that they involve a simultaneous measurement of the charge and current densities. As a result they are not subject to explanations involving odd-even effects or mass difference effects. Thus, a systematic difference between the measured charge and current radius is seen over a wide range of nucleon number.

F. States between 3.0 and 4.0 MeV

Figure 14 shows the known excited states of ^{92}Mo below 4 MeV where spin and parity assignments have been established. Also shown are the excitation spectra of the SM and BP. Below 3 MeV both calculations do a reasonable job of predicting the spins and parities of the observed levels. Between 3 and 4 MeV the calculations differ considerably and the BP calculation predicts only one state, a 2^+ state around 3.93 MeV. This indicates that the structure of the states in this region is complicated and, in general, dominated by 2p-2h components relative to the ground state. For example, the positive-parity

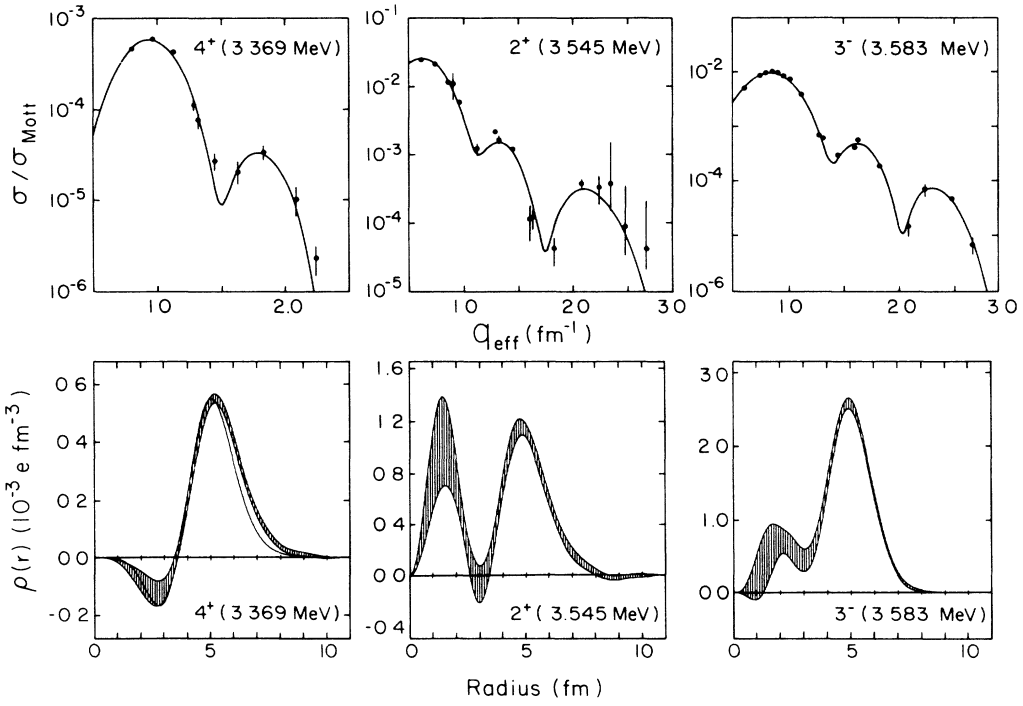

FIG. 16. Form factors and transition charge densities for the states at 3.369 MeV ($J^\pi=4^+$), 3.545 MeV ($J^\pi=2^+$), and 3.583 MeV ($J^\pi=3^-$). The curves in the form factor plots are the DWBA fits as described in the text. The solid curve for the density of the 3.369-MeV level is a two-component SPM fit to the data.

states between 3 and 4 MeV are probably built from configurations like

$$\pi[(1g_{9/2}^2)_{2^+}\otimes(1g_{9/2}^2)_{2^+}]_{J^+}$$

and

$$\pi[(2p_{1/2}2p_{3/2}^{-1})_{2^+}\otimes(1g_{9/2}^2)_{2^+}]_{J^+}\ .$$

Similarly, negative-parity two-phonon states can arise by coupling a 3^- or 5^- excitation with a 2^+ excitation. The SM wave functions support this observation. Since, in electron scattering, we only observe the one-body densities one would expect low cross sections for these 2p-2h states.

In this experiment we measured cross sections for seven states between 3 and 4 MeV. In general, the cross sections were all small and the backward scattering data showed little transverse strength. The data probably reveal the smaller 1p-1h components of these states and indicate the extent of mixing between the 1p-1h and 2p-2h components. Identification of all the states discussed below relied heavily on three sources of information: Nuclear Data Sheets,[38] a thesis by E. J. Kaptein[39] describing a high-resolution (p,p') experiment, and a table of excited states observed in the $(\alpha,\alpha'\gamma)$ reaction.[40]

1. The 2^+ state at 3.092 MeV

The form factor for this state is shown in Fig. 15. Also shown in Fig. 15 is the transition charge density extracted for this state. The data are consistent with the absence of a transition current density although a small current density does improve the fit slightly.

The SM prediction for this state is shown with the experimental density. Judging by the strong disagreement with experiment, the calculation provides no insights on this state. The experimental density is very nearly the same shape as the density for the first 2^+ state and therefore probably has a strong $\pi 1g_{9/2}\rightarrow 1g_{9/2}$ component. The SM wave function is suggestive of configurations in which there are two pairs each coupled to 2^+. The energy of this state being very close to twice that for the first 2^+ state suggests a

$$\pi[(1g_{9/2}^2)_{2^+}\otimes(1g_{9/2}^2)_{2^+}]_{2^+}$$

coupling.

2. The $L=4$ state at 3.369

The state at 3.369 has been observed before in (p,p') and $(\alpha,\alpha'\gamma)$ reactions. In the $(\alpha,\alpha'\gamma)$ reaction an $L=4$ assignment was made with a tentative negative-parity assignment. The (p,p') reactions were consistent with the $L=4$ assignment.

Figure 16 shows the form factor and the fitted density for this state. The fact that this state was observed in forward scattering and not at 155° practically rules out a 4^- assignment. The fit was done assuming $J^\pi=4^+$ using FBE and SPM transition density models. The good fit indicates that this assignment is probably correct. The SPM density is a combination of two components, $\pi(1g_{9/2},1g_{9/2}^{-1})_{4^+}$ and $\pi(2d_{5/2},1g_{9/2}^{-1})_{4^+}$. The amplitudes of the two components were fit and were found to be 0.08

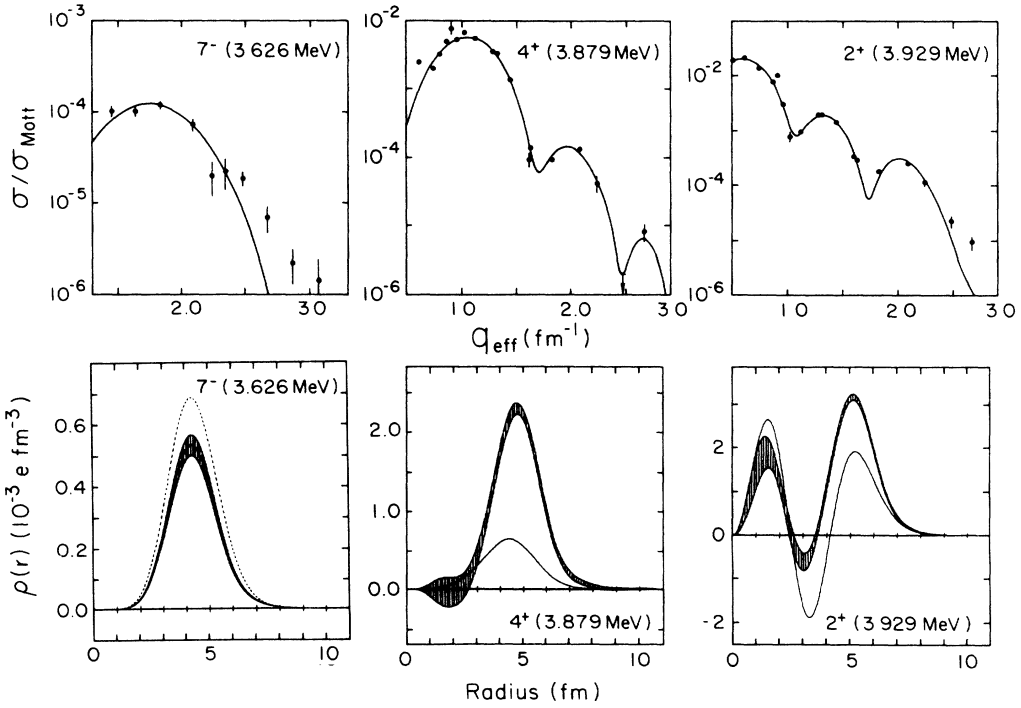

FIG. 17. Form factors and transition charge densities for the states at 3.626 MeV ($J^\pi=7^-$), 3.879 MeV ($J^\pi=4^+$), and 3.925 MeV ($J^\pi=2^+$). The curves in the form factor plots are best-fit DWBA calculations while the model predictions for the densities as described in the text are given in the lower set of figures.

and 0.12, respectively. The node in the density is indicative of a transition between orbitals of different oscillator shells.

3. The 2^+ state at 3.545 MeV

The 3.545-MeV state was only weakly excited in our experiment. The shape of the transition charge density is very similar to the shape obtained for the state at 3.929 MeV, the fourth 2^+ state.

4. The 3^- state at 3.583 MeV

The form factor for the 3^- state at 3.583 MeV is shown in Fig. 16. The shape of the density resembles that for the 3_1^- and 5_1^- states. The weak transition strength indicates it is probably of the two-phonon type. No indication of transverse strength was observed.

5. The 7^- state at 3.626 MeV

This state has been observed before in the studies of the high spin metastable states of ^{92}Mo. The cascade $11^-\rightarrow 9^-\rightarrow 7^-\rightarrow 5^-\rightarrow 3^-$ was observed after ^{64}Ni and ^{65}Cu were bombarded with ^{32}S at 132 MeV. The SM calculation predicts a 7^- state at nearly this energy (3.370 MeV) and with a configuration suggestive of a

$$\pi(1g_{9/2},1f_{5/2}^{-1})_{5^-}\otimes(2^+)$$

coupling. The fit shown in Fig. 17 was done by fitting the density obtained for the 7_2^- (4.560-MeV) state to the data for the 7_1^- state. The amplitude for this fit is 0.163 ± 0.031 and can be used as a measure of the mixing between 1p-1h and 2p-2h components. Also shown with the density are two curves. The solid curve is a fit using the SPM and a single component, $\pi(1g_{9/2},1f_{5/2}^{-1})$, for the density. Only the amplitude with the result 0.11 ± 0.03 is fit. The dashed curve is the SM prediction.

6. The 4^+ state at 3.879

This state has an order-of-magnitude larger cross section than the state at 3.369 MeV. The shape of the density is very similar to the 4_1^+ density, shown as a solid line in Fig. 17, and indicates a large $\pi(1g_{9/2},1g_{9/2}^{-1})$ component to the transition.

7. The 2^+ state at 3.929 MeV

The BP calculation predicts a 2^+ state at 3.930 MeV. The predicted density for this state has approximately equal amplitudes for the

$$\pi(2p_{1/2},2p_{3/2}^{-1}),$$

$$\pi(2p_{1/2},1f_{5/2}^{-1})$$

and

$$\pi(1g_{9/2},1g_{9/2}^{-1})$$

components. In addition, there is a strong $\nu(2d_{5/2},1g_{9/2}^{-1})$ component. The shape of the experimental density in Fig. 17 is very similar to that for the 2_2^+ (3.307-MeV) state in ^{90}Zr and the 2_1^+ (1.836-MeV) state in ^{88}Sr. The shape of the BP density (solid line) is qualitatively correct and is also of roughly the right magnitude. This suggests that the state in ^{90}Zr (and ^{92}Mo) is a pair (two pair) of protons coupled to a ^{88}Sr core in its first excited state.

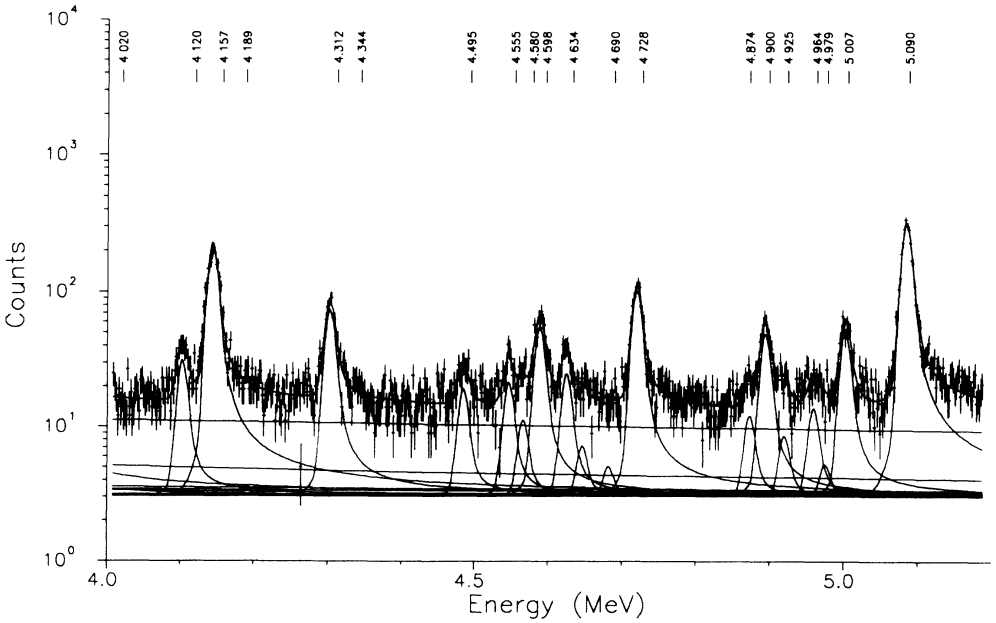

FIG. 18. Spectrum of scattered electrons for the excitation region 4.0–5.3 MeV. The energies listed above the spectrum indicate the levels which have been included in the peak shape fits.

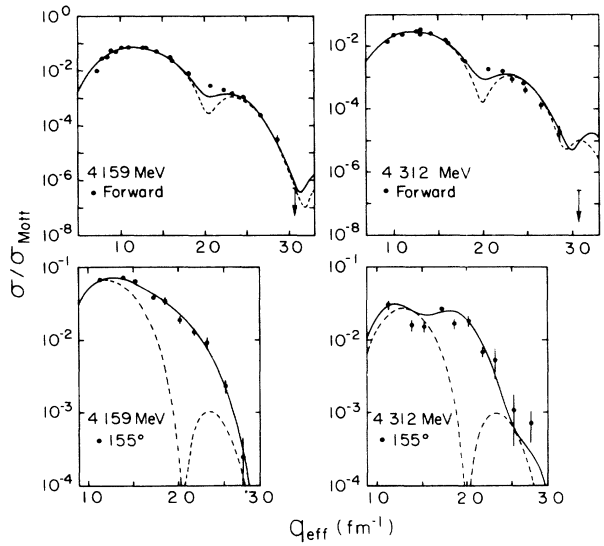

FIG. 19. Form factors for the 5^- states at 4.159 and 4.312 MeV. Solid curves are best-fit DWBA calculations while the dashed curves show the longitudinal contribution.

G. States between 4.0 and 5.2 MeV

The density of excited states increases rapidly above 4.0 MeV. Neutron pickup reactions on ^{91}Zr indicate that neutron 1p-1h states in ^{90}Zr begin to appear at an excitation energy of 4.2 MeV. The same situation applies to ^{92}Mo. The positive-parity states based on the $\nu(2d_{5/2}, 1g_{9/2}^{-1})$ configuration should occur in this excitation region and, in part, account for the increased level density.

Figure 18 shows a fitted electron spectrum for this excitation region. Above the spectrum are listed the energies at which peaks were included in the peak shape fits.

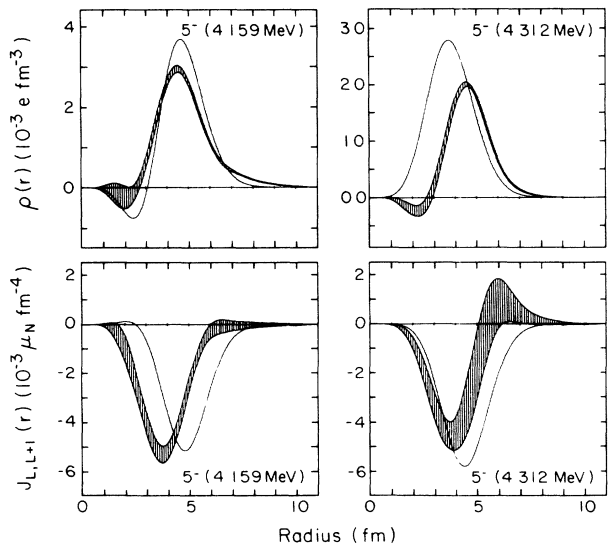

FIG. 20. Densities extracted for the 5^- states at 4.159 and 4.312 MeV. Solid curves are BP predictions.

The state at 4.555 MeV has been discussed in a previous section. The two states at 4.690 and 4.925 have backward scattering form factors which indicate that they have unnatural parity and will be discussed in the next section on magnetic transitions. Three states in this region for which form factors could be extracted are discussed here. Additional spectroscopy is reported elsewhere.[41]

1. *The 5^- states at 4.159 and 4.312 MeV*

These levels have been observed previously in (p,p') and $(\alpha,\alpha'\gamma)$ reactions. The state at 4.159 is actually a doublet of a 4^+ state at 4.144 MeV and a 5^- state at 4.159 MeV. The two states are unresolved in this experiment. The peak positions and widths in all spectra are

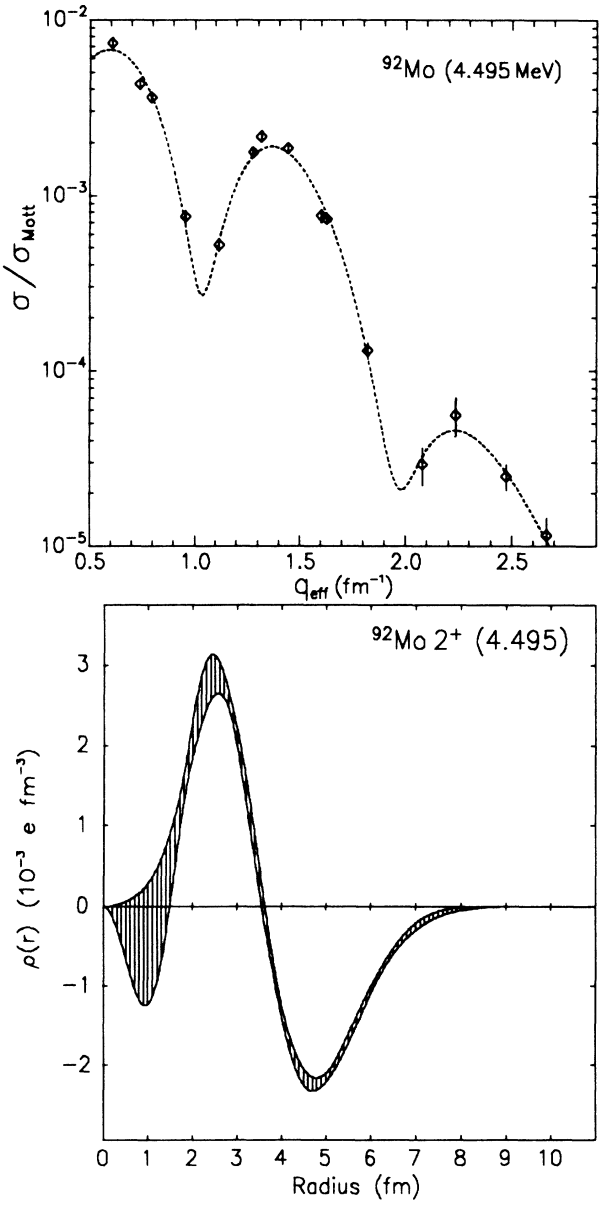

FIG. 21. Form factor and transition charge density for the 2^+ state at 4.495 MeV.

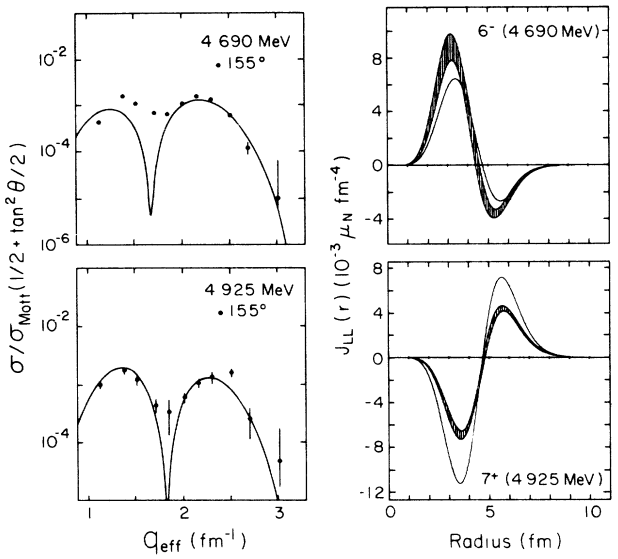

FIG. 22. Form factors for the states at 4.690 and 4.925 MeV. Also shown are the transition current densities for these excitations and the BP predictions for the first 6^- and 7^+ states.

consistent with all strength coming from the 5^-.

The BP calculation predicts the second and third 5^- states at 4.323 and 4.549 MeV. A 4^+ state which is almost a pure $\nu(2d_{5/2}, 1g_{9/2}^{-1})$ configuration is predicted at 4.290 MeV. If the 4^+ state of this doublet corresponds to the neutron 1p-1h state one would expect a rather small (e,e') cross section. This might explain why there is little evidence for the 4.159 MeV state being a doublet. These BP 5^- states are dominated by $\pi(1g_{9/2}, 1f_{5/2}^{-1})$ and $\pi(1g_{9/2}, 2p_{3/2}^{-1})$ components, the two states being roughly orthogonal mixtures of the two components.

Figure 19 shows the form factors for the two levels and the DWBA fits which were done assuming $J^\pi = 5^-$ for both states. Simultaneous fits were done to the forward and backward scattering data. The densities corresponding to these fits are shown in Fig. 20. Also shown are the densities from the BP calculation.

2. *The 2^+ state at 4.495 MeV*

Figure 21 shows the form factor and transition density for the 2^+ state at 4.495 MeV. The shape of the density indicates a transition between orbitals of different oscillator shells. The most likely 1p-1h components are $\pi(2p_{1/2}, 1f_{5/2}^{-1})$ and $\pi(2d_{5/2}, 1g_{9/2}^{-1})$. The BP calculation predicts 2^+ states at 4.479 and 4.874 MeV. The state at 4.479 MeV has a dominant component of $\pi(2p_{1/2}, 2p_{3/2}^{-1})$. From Eq. (3.6) the dominant term in the density is given by the $2p$ radial wave function squared. Unlike the measured density, this shape will not have a node. The density for the 4.874-MeV BP state (not shown) has a shape which resembles the measured density but which peaks at a larger radius. This BP state has a dominant component of $\pi(2d_{5/2}, 1g_{9/2}^{-1})$. The shape of the experimental density favors a strong $\pi(2p_{1/2}, 1f_{5/2}^{-1})$ component and therefore does not correspond well with either of the BP states.

H. The states at 4.690 and 4.925 MeV

The backward scattering data between 4.0 and 5.3 MeV show two unidentified states at 4.690 and 4.925 which have transverse form factors peaking at large momentum transfer. This signature is characteristic of unnnatural-parity high spin states. By analogy with the ^{90}Zr data, these states can be tentatively identified as a 6^- state (4.690 MeV) and a 7^+ state (4.925 MeV).

The data for these states are shown in Fig. 22 along with the fits to the $M6$ and $M7$ form factors. Both fits were done to the backward scattering data alone using the SPM. The form of the density for the 6^- state was taken to be

$$\alpha\pi(1g_{9/2}, 1f_{5/2}^{-1}) + \beta\pi(1g_{9/2}, 2p_{3/2}^{-1}) .$$

For the 7^+ fit a single component $\nu(2d_{5/2}, 1g_{9/2}^{-1})$ was used.

Both states appear to be unresolved from nearby states. The low-q forward scattering data (not shown) indicate an excess cross section indicative of a nearby natural-parity state while the high-q forward scattering data agree well with the fits. A known 3^- state at 4.920 MeV is the most likely source of the excess cross section for the possible 7^+ state. While several states near 4.690 MeV have been identified in the (p,p') reaction, the spin and parity of these states have not been established. Further analysis and/or additional data are necessary to extract the magnetization densities in FBE; the densities shown in Fig. 22 were extracted in the SPM discussed above. BP predictions for the first 6^- and 7^+ states have excitation energies of 4.624 and 4.778 MeV, respectively.

VI. SUMMARY AND CONCLUSIONS

In this experiment differential cross sections have been measured for over 30 states in ^{92}Mo. The determination of the ground-state charge density has been improved by extending the range of momentum transfer to 3.1 fm^{-1}. This improvement allows a more accurate determination of the ground-state charge difference between ^{90}Zr and ^{92}Mo. In particular, the difference has been determined well into the nuclear interior where structure is observed similar to that predicted in an HF-DME calculation.

We have identified a strongly excited 7^- state at 4.555 MeV. Two other high spin states 4.690 and 4.925 MeV have also been observed and tentatively been identified as 6^- and 7^+ states, respectively. These three states should provide useful information for establishing single-particle energies used in model calculations. The state at 3.369 MeV, previously given a tentative spin-parity assignment of 4^-, now can be identified as a 4^+.

The densities for the 2^+ to 8^+ multiplet have now been accurately determined for both ^{90}Zr and ^{92}Mo. Both of the calculations used for comparison here do not include enough collectivity to account for the strength of the $E2$ transition. At the same time both calculations overpredict the strength of the $E8$ transition to the 8^+ state which has been shown to have very little collectivity. The densities all arise from the same dominant configuration, but with differing amounts of core polar-

ization depending on the multipolarity. Correctly predicting the densities for all four states would be a stringent test for model calculations.

The transition densities for the 3^- state at 2.850 MeV also provide useful information on the collectivity which must be included in a realistic model. A non-negligible transition current density has been measured for this state. Correctly predicting both the charge and the current densities requires a correct mixture between single particle and collective degrees of freedom.

The comparison of the $E5$ transition strengths has been extended to ^{92}Mo. The quenching of the transition current relative to the transition charge was again observed. The analysis of the ^{92}Mo data further supports the idea that the quenching is due to backward going particle-hole amplitudes. The quenching factors determined for ^{89}Y, ^{90}Zr, and ^{92}Mo provide a direct measure of ground-state occupations.

Finally, the most intriguing data comes from the particle-hole 7^- state at 4.555 MeV. The particle-hole states based on the $\pi(1g_{9/2}, 1f_{5/2}^{-1})$ configuration have now been identified in ^{88}Sr, ^{90}Zr, and ^{92}Mo. In all three nuclei the strength of the transition for both the current and charge densities is significantly less (20–30 %) than would be found for a pure particle-hole transition. This quenching is as yet unexplained and very surprising for a state which should have a simple configuration. Another interesting feature of this state is that the transition current density peaks farther into the nuclear interior than is expected. A fit using the SPM and a single component for the density does not provide a good fit to both the forward scattering and backward scattering data. If a separate radius parameter is fit for the current-density calculation, a good fit can be achieved. Again, this is unexplained and neither the quenching nor the radius shift seem to be within the scope of the conventional nuclear models employed in this analysis.

[1]O. Schwentker, J. Dawson, J. Robb, J. Heisenberg, J. Lichtenstadt, C. N. Papanicolas, J. Wise, J. S. McCarthy, L. T. van der Bijl, and H. P. Blok, Phys. Rev. Lett. **50**, 15 (1983).

[2]O. Schwentker, J. Dawson, S. McCaffrey, J. Robb, J. Heisenberg, J. Lichtenstadt, C. N. Papanicolas, J. Wise, J. S. McCarthy, N. Hintz, and H. P. Blok, Phys. Lett. **112B**, 40 (1982).

[3]J. Heisenberg, J. F. Dawson, T. Milliman, O. Schwentker, J. Lichtenstadt, C. N. Papanicolas, J. Wise, J. S. McCarthy, N. Hintz, and H. P. Blok, Phys. Rev. C **29**, 97 (1984).

[4]T. E. Milliman, J. H. Heisenberg, F. W. Hersman, J. P. Connelly, C. N. Papanicolas, J. E. Wise, H. P. Blok, and L. T. van der Bijl, Phys. Rev. C **32**, 805 (1985).

[5]W. Bertozzi, M. V. Hynes, C. P. Sargent, W. Turchinetz, and C. Williamson, Nucl. Instrum. Methods **162**, 211 (1979).

[6]W. Bertozzi, M. V. Hynes, C. P. Sargent, C. Cresswell, P. C. Dunn, A. Hirsh, M. Seitch, B. Norum, F. N. Rad, and T. Sasanuma, Nucl. Instrum. Methods **141**, 457 (1977).

[7]F. W. Hersman, Ph.D. thesis, Massachusetts Institute of Technology, 1983.

[8]J. J. Kelly, C. E. Hyde-Wright, and F. W. Hersman, ALLFIT computer code, unpublished.

[9]J. Bergstrom, in *MIT 1967 Summer Study, Medium Energy Nuclear Physics with Electron Accelerators* (MIT, Cambridge, Massachusetts, 1967), p. 251.

[10]B. Dreher, Ph.D. thesis, Universität Mainz, 1974.

[11]Phan Xuan Ho, J. B. Bellicord, A. Bussiere, Ph. Leconte, and M. Priou, Nucl. Phys. **A179**, 529 (1972).

[12]R. P. Singhal, S. W. Brain, C. S. Curran, T. E. Drake, W. A. Gillespie, A. Johnston, and E. W. Lees, Nucl. Phys. **A216**, 29 (1973).

[13]J. Heisenberg, Adv. Nucl. Phys. **12**, 61 (1981).

[14]J. Heisenberg and H. P. Blok, Annu. Rev. Nucl. Part. Sci. **33**, 569 (1983).

[15]G. G. Simon, C. Schmitt, F. Borkowski, and F. W. Walther, Nucl. Phys. **A333**, 381 (1980).

[16]W. Bertozzi, J. Friar, J. Heisenberg, and J. W. Negele, Phys. Lett. **41B**, 408 (1972).

[17]W. C. Haxton, private communication. See also M. M. Gazzaly, N. M. Hintz, M. A. Franey, J. Dubach, and W. C. Haxton, Phys. Rev. C **28**, 294 (1983).

[18]K. Allaart, private communication; K. Allaart, E. Boeker, G. Bonsignori, M. Savoia, and Y. K. Gambhir, Phys. Rep. **169**, 209 (1988); K. Allaart and E. Boeker, Nucl. Phys. **A168**, 630 (1971).

[19]J. W. Negele and D. Vautherin, Phys. Rev. C **5**, 1472 (1972).

[20]H. Überall, *Electron Scattering from Complex Nuclei* (Academic, New York, 1971).

[21]R. Engfer, J. Schneuwly, J. L. Vuilleumier, H. K. Walter, and A. Zehnder, At. Data Nucl. Data Tables **14**, 509 (1974).

[22]B. Dreher, J. Friedrich, K. Merle, and G. Lührs, Nucl. Phys. **A235**, 219 (1974).

[23]J. M. Cavedon, B. Frois, D. Goutte, M. Huet, Ph. Leconte, X. H. Phan, S. K. Platchkov, C. N. Papanicolas, S. E. Williamson, W. Boeglin, I. Sick, and J. Heisenberg, Phys. Rev. Lett. **58**, 195 (1987).

[24]J. Heisenberg, Comments Nucl. Part. Phys. **13**, 267 (1984).

[25]G. Vourvopoulos and J. D. Fox, Phys. Rev. **177**, 1558 (1969).

[26]M. R. Cates, J. B. Ball, and E. Newman, Phys. Rev. **187**, 1682 (1969).

[27]J. H. Heisenberg, unpublished.

[28]K. T. Knöpfle, M. Rogge, C. Mayer-Böricke, J. Pedersen, and D. Burch, Nucl. Phys. **A159**, 642 (1971).

[29]J. Piccard and G. Bassani, Nucl. Phys. **A131**, 636 (1969).

[30]R. L. Kozub and D. H. Youngblood, Phys. Rev. C **4**, 535 (1971).

[31]B. M. Preedom, E. Newman, and J. C. Hiebert, Phys. Rev. **166**, 1156 (1968).

[32]J. W. A. den Herder, H. P. Blok, E. Jans, P. H. M. Keiser, L. Lapikas, E. N. M. Quint, G. van der Steenhoven, and P. K. A. de Witt Huberts, Nucl. Phys. **A490**, 507 (1988).

[33]L. T. van der Bijl, Ph.D. thesis, Vrije Universiteit, 1982.

[34]P. Luksch, Nuclear Data Sheets, **30**, 638 (1980).

[35]P. X.-Ho, J. Bellicard, Ph. Leconte, and I. Sick, Nucl. Phys. **A210**, 189 (1973).

[36]S. Platchkov, J. B. Bellicard, J. M. Cavedon, B. Frois, D.

Goutte, M. Huet, P. Leconte, Phan Xuan Ho, P. K. A. de Witt Huberts, L. Lapikas, and I. Sick, Phys. Rev. C **25**, 2318 (1982).
[37]A. M. Selig, I. E. Zacharov, P. K. A. de Witt Huberts, and S. K. Platchkov, Phys. Lett. **162B**, 251 (1985).
[38]P. Lucksch, Nucl. Data Sheets **30**, 573 (1980).
[39]E. J. Kaptein, Ph.D. thesis, Vrije Universiteit, 1978.
[40]R. Klein, Ph.D. thesis, Heidleberg, 1984.
[41]T. E. Milliman, Ph.D. thesis, University of New Hampshire, 1987.